Appl. Phys. A 78, 465–469 (2004)
DOI: 10.1007/s00339-003-2405-0

Applied Physics A
Materials Science & Processing

P.C.M. PLANKEN[1]
H.J. BAKKER[2,✉]

Towards time-resolved THz imaging

[1] Delft University of Technology, Faculty of Applied Sciences, Department of Applied Physics, Lorentzweg 1, 2628 CJ Delft, The Netherlands
[2] FOM-Institute AMOLF, Kruislaan 407, 1098 SJ Amsterdam, The Netherlands

Received: 6 August 2003/Accepted: 18 September 2003
Published online: 14 January 2004 •

ABSTRACT We describe a setup that allows for the measurement of high-quality images at frequencies in the far-infrared (THz) regime of the spectrum. By using water-cooled THz emitters that are biased with a 50-kHz, ±400-V square wave, rapid delay scanning, and differential lock-in detection at 50 kHz, we attain shot-noise-limited detection of THz transients. As a result, THz transients with a large dynamic range of ~ 5000 can be measured in 20 ms. We show that the THz imaging setup enables the time-resolved detection of the diffusion of gases.

PACS 07.57.-c; 42.30.-d; 95.85.Gn; 36.20.Ng

1 Introduction

An important advantage of far-infrared or terahertz (1 THz = 10^{12} Hz) radiation is that it can easily penetrate objects that are opaque to visible light, like books, bandages, and wallets, and can thus be used to look inside these objects. In addition, THz radiation has the advantage that it is non-ionising, because a THz photon has an extremely small energy content. Nevertheless, up to recently, THz spectroscopy has hardly been used for real-world spectroscopic applications, mainly due to a lack of suitable sources and detectors. Most detectors, for example, require liquid-helium cooling, because at room temperature their response is dominated by background thermal radiation.

In recent years the field of terahertz spectroscopy has been strongly stimulated by the development of new efficient methods to generate and detect far-infrared radiation. The new sources are all based on the partial conversion of ultra-short visible or near-infrared laser pulses to broadband far-infrared radiation. For instance, the frequency components in the bandwidth of an ultra-short laser pulse can be mixed in a non-linear crystal, such as ZnTe or GaP, to generate a few-cycle THz pulse [1–3]. This process is denoted as non-resonant optical rectification. In another method, an ultra-short laser pulse illuminates a semiconductor such as GaAs biased with an electric or a magnetic field, giving rise to an ultra-fast current transient which emits a THz pulse [4–6]. In this latter method, microfabrication techniques are used to create electrodes separated by only a few to tens of microns.

An essential step forward in the detection of THz radiation has been the development of time-gated methods that allow for a dramatic reduction of the background thermal radiation. The most commonly used time-gated methods are in fact the reverse of the above-described methods of generation. For instance, THz pulses can be detected by electro-optic sampling, which is the reverse of non-resonant optical rectification. In this process, the THz electric field induces a polarisation change in the optical field of a synchronised probe pulse in a crystal such as (110)-oriented ZnTe [7–9]. In another method, THz light is detected with microfabricated antennas on semiconductors, such as low-temperature-grown GaAs (LT-GaAs) or radiation-damaged Si on sapphire, that are time gated by a synchronised probe pulse [4, 10]. Electro-optic detection is inherently simple, but multiple reflections in the detection crystal, and reshaping of the THz pulse due to phase matching and absorption, can lead to a severe distortion of the THz pulse [11, 12]. Time-gated microfabricated antennas, on the other hand, in general require clean-room facilities to make them.

In this paper we show that shot-noise-limited detection of THz transients can be attained by combining quasi-large-aperture, semi-insulating GaAs (SI-GaAs) emitters with electro-optic detection. We demonstrate that the high signal to noise ratio of this system enables efficient and relatively fast THz imaging.

2 Experimental

The THz pulses are generated by focusing 200 mW of the light of a femtosecond Ti : sapphire oscillator to a spot with a diameter of 120 μm (FWHM) on a piece of semi-insulating GaAs (MCP Wafer Technology Ltd.). The Ti : sapphire laser has been obtained from Femtolasers Produktions, Austria, and produces 15-fs pulses with a centre wavelength of 775 nm at a repetition rate of 72 MHz. The SI-GaAs wafer has a dark resistivity of more than 5×10^7 Ω cm. On the surface of the wafer, two crescent-shape silver-paint electrodes are painted with a smallest separation of 0.4 mm. The sample is glued with silver paint onto two 2-mm-thick and 1-cm-wide copper strips, separated by 2 mm. Each copper strip forms a contact to one silver-paint electrode only.

✉ E-mail: h.bakker@amolf.nl

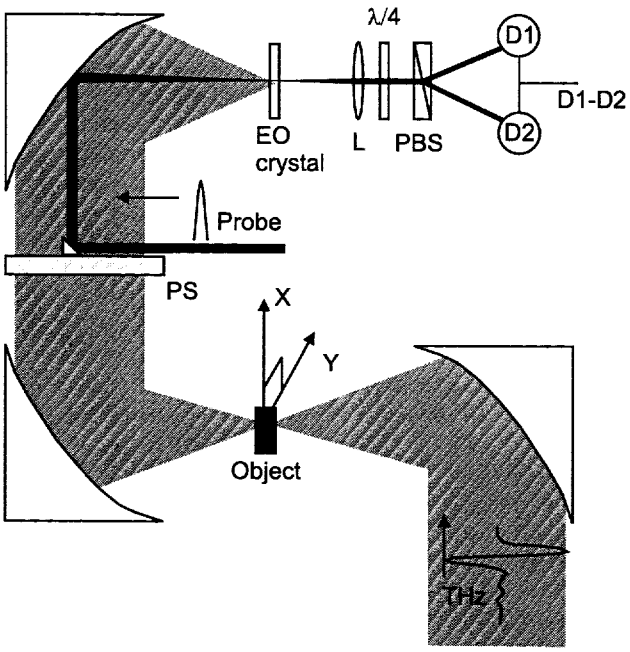

FIGURE 1 Experimental setup used for THz imaging spectroscopy

The copper strips serve as electrical contacts to the voltage source and provide a good heat sink. The copper strips are connected to a water-cooled copper block using an electrically isolating but thermally conductive sheet with a width of 200 μm. This sheet is made from coated glass fibre with a specially loaded silicone compound (Warth International Ltd., Kool Pads K200). We found that keeping the crystal at a temperature of approximately 20 degrees strongly increases the emitted THz amplitude. We applied a 50-kHz, square-wave ac bias voltage with an amplitude of 400 V to the emitter. When the voltage changes from −400 V to +400 V, the THz signal also changes sign. Hence, when lock-in detection is used, the measured signal is twice the signal that would be obtained when the applied voltage is switched between 0 and 400 V. This method to increase the measured signal without increasing the THz amplitude is quite similar to the method of polarisation modulation recently reported for a system based on a ZnTe THz emitter [13]. The emitted THz radiation is collimated using a silicon hyperhemispherical lens that is glued onto the back of the crystal.

The optical path of the generated vertically polarised THz beam is shown in Fig. 1. The THz beam is focused with a gold-coated paraboloidal mirror with a focal length of 10 cm onto an object. After the object, the THz beam is recollimated by a second gold-coated paraboloidal mirror with a focal length of 10 cm and passes through a 2-mm-thick piece of polystyrene foam. The polystyrene foam has a refractive index of 1.017 and an absorption coefficient of less than 1 cm^{-1} for frequencies below 4 THz, and is thus nearly completely transparent in this range [14]. A small, gold-coated, right-angle prism is glued onto the foam. This prism is used to collinearly combine the THz pulse with a time-delayed, horizontally polarised probe pulse. Both the THz beam and the probe beam are focused onto a 1-mm-thick, (110)-oriented ZnTe crystal or a 0.1-mm-thick, (110)-oriented GaP crystal with a third gold-coated paraboloidal mirror with a focal length of 5 cm. The probe beam then passes through a quarter-wave plate and a Wollaston prism. The Wollaston prism separates the two orthogonal polarisation components of the probe beam, which are subsequently focused onto a home-built differential detector. When there is no THz electric field present, both polarisation components have the same intensity and the signal from the differential detector is zero. The THz electric field changes the polarisation of the probe pulse in the electro-optic crystal from linear to slightly elliptical, and thereby induces a signal that is proportional to the electric field. By changing the optical delay between the probe pulse and the THz pulse, the complete electric field of the THz pulse is measured. The time delay is varied by passing the probe beam over a mirror that is attached to the cone of a conventional speaker that is driven with a frequency of 50 Hz. Each delay-time scan has a range of approximately 35 ps and consists of 1024 different delay-time points. The setup is enclosed in a box that is purged with dry nitrogen gas to reduce the effects of water-vapour absorption. It can be shown that this system allows for shot-noise-limited detection of THz transients [15].

To measure images, the object is moved in the directions perpendicular to the THz beam using conventional x, y stepper-motor translation stages. With these stages, the object can be translated over a total area of 4 cm^2 × 4 cm^2. The images to be presented below consist either of 70 × 70 or 160 × 140 different x, y positions (pixels). Both the data collection at a pixel and the moving of the x, y stages to new positions take approximately 0.1 s.

3 Results and discussion

Figure 2 shows the THz electric field that is measured using a 1-mm-thick ZnTe electro-optic detection crystal. The data shown are obtained in a single delay scan and are measured in 20 ms. Some weak oscillations are observed for longer delays that are caused by absorption of residual water

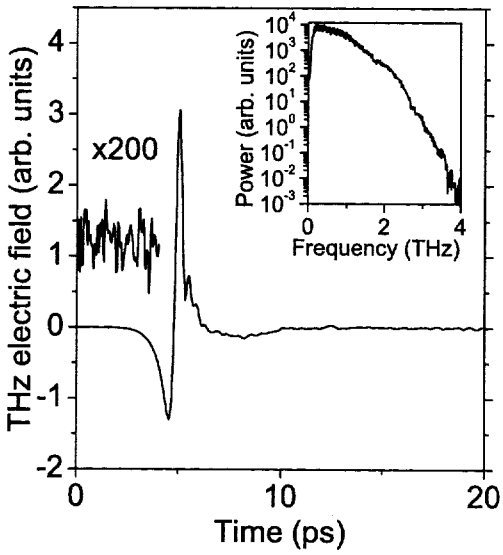

FIGURE 2 Measured THz electric field using a 1-mm ZnTe electro-optic crystal. In the *inset* the corresponding spectrum is shown

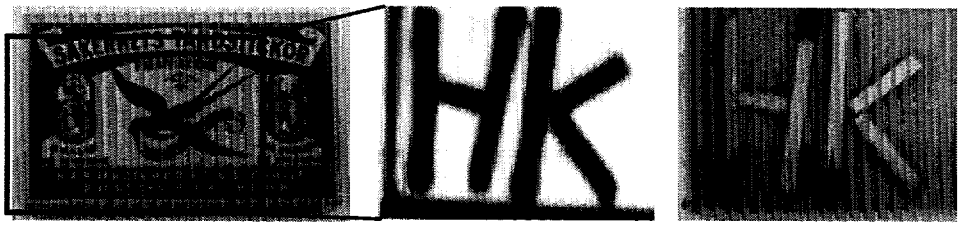

FIGURE 3 Illustration of the potential of THz imaging. In the *left-hand panel* an optical picture of a matchbox is shown that is not transparent to light in the optical region of the spectrum. If the same matchbox is imaged with THz light (*middle panel*), the object hidden in the matchbox is revealed. This image is compared with a picture of the same part of the opened matchbox (*right-hand panel*)

vapour in the nitrogen atmosphere. In the inset of Fig. 2 the corresponding spectrum is presented. The THz pulse peaks at approximately 0.5 THz. At 1.7 THz and 2.9 THz weak absorptions are observed that result from the absorption by residual water vapour.

The amplitude of the THz electric field can be calculated from the difference $\Delta P = P_1 - P_2$ in intensity on the two diodes of the differential detector. If $P_{\text{probe}} = P_1 + P_2$ is the intensity of the probe beam, the measured signal in terms of $\Delta P/P_{\text{probe}}$ is related to the THz electric field E_{THz} by

$$\frac{\Delta P}{P_{\text{probe}}} = \frac{\omega n^3 E_{\text{THz}} r_{41} L}{c}. \tag{1}$$

In this equation, $r_{41} = 3.9$ pm/V is the electro-optic coefficient, $n = 2.8$ the near-IR refractive index, c the speed of light, ω the near-IR angular frequency, and L the length of the crystal. $\Delta P/P_{\text{probe}} = 7 \times 10^{-3}$, from which it follows that the peak THz electric field is approximately 98 V/cm. The corresponding THz power measured with a pyroelectric detector is estimated to be 100 μW.

The dynamic range of the THz measurement can be defined by the ratio of the maximum THz electric field and the root mean square width of the baseline (background) fluctuations. Using this definition, the dynamic range is ~ 5000 for the measurement shown in Fig. 2. This dynamic range represents the maximum contrast (ratio of the maximum and minimum resolvable transmission) of the imaging setup. The minimum difference in absorption of different points of the image that can be detected is determined by the magnitude of the amplitude fluctuations. For the settings we use in the imaging (taking an average of five or seven delay-time scans), we find that the root mean square width of the peak amplitude is approximately 1%, which thus represents the lower limit for the absorption differences that can be resolved.

In Fig. 3 the potential of THz imaging in finding hidden objects is illustrated. Clearly, the matchbox that is completely opaque at optical frequencies becomes transparent in the far infrared, and turns out to conceal the initials of a well-known physicist. The THz image consists of 160 pixels × 140 pixels and has a size of 4×3.08 cm^2. The signal at each pixel is an average over seven delay scans, and represents the value of the maximum of the THz transient measured at that pixel. The total measurement time of the image is 4500 s, and the resolution attained is approximately 500 μm.

In Fig. 4 THz electric fields are shown that are measured using a 0.1-mm-thick GaP electro-optic detection crystal. Both a reference signal (no object) and the signal obtained

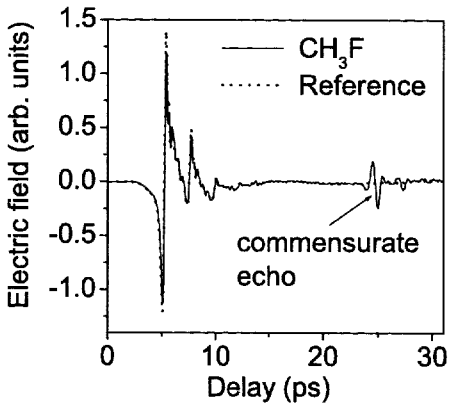

FIGURE 4 Measured THz electric fields using a 0.1-mm GaP electro-optic crystal. The *solid curve* represents the THz electric field transmitted through CH_3F gas. The *dashed curve* represents the input THz electric field

after propagation through a gas cell (with a length of 7 cm) containing CH_3F gas (~ 100 mbar), are shown. The signals are the result of a single delay scan and are measured in 20 ms. The measured signal is much smaller ($\Delta P/P_{\text{probe}} = 3.5 \times 10^{-4}$) than the signal measured with a 1-mm ZnTe electro-optic detection crystal. However, an important advantage of using 0.1-mm-thick GaP is that the spectrum of the THz radiation extends to higher frequencies. In Fig. 5 it is demonstrated that with 0.1-mm-thick GaP frequency components up to 6 THz can be detected.

The signals shown in Fig. 4 show several recurrences (at ~ 7.5, 10, and 12.5 ps) that result from multiple THz reflections in the GaP crystal. These recurrences show small modulations that are caused by weak, high-frequency absorption lines of residual water vapour. In the spectrum of the THz signal shown in Fig. 5 the effect of the multiple reflections in the GaP crystal shows up as etalon oscillations with a period of 0.45 THz.

In addition to the etalon oscillations, the spectrum of the THz signal propagated through CH_3F gas shows sharp dips that are due to rotational absorptions of the CH_3F molecules [16]. In the time domain, these absorptions appear as recurrences of the THz signal at distinct long-time delays. These recurrences are generated as a result of the coupling of the propagating THz light with the rotational resonances of the gas and have been denoted in the literature as commensurate echoes [17]. These echoes are the result of a linear optical effect and should not be confused with photon echoes that are generated as a result of a non-linear (at least third-order) optical interaction. The time delays of the commensurate echoes

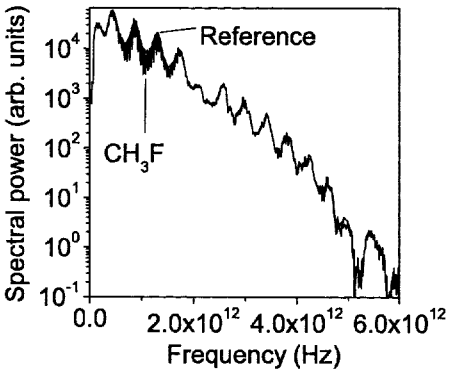

FIGURE 5 Spectra corresponding to the THz transients of Fig. 4. The spectra show modulations due to multiple reflections in the GaP electro-optic crystal. The spectrum of the THz field propagated through CH_3F gas shows additional sharp absorption lines due to rotational absorptions of the CH_3F molecules

are determined by the frequency spacing of the rotational absorption lines. In Fig. 4 the first commensurate echo is observed at a delay of ~ 25 ps.

As an illustration of the ability of our setup to perform time-resolved THz imaging, we show measurements on the real-time diffusion of the gas CH_3F through a 2-cm-thick block of polystyrene foam. In this experiment we drilled a hole with a width of 2 mm in which we positioned a hollow needle. The needle was pressurised with CH_3F at 1.5 bar. To prevent gas leakage along the needle, the opening surrounding the needle was sealed with epoxy. In Fig. 6 five images of the spatial distribution of CH_3F gas in the polystyrene foam are shown that are taken at different times after the inflow of the gas. The five images represent a two-dimensional projection of the diffusion of the CH_3F gas through the polystyrene foam. The total measurement time of each image is 500 s. The signal at each pixel is an average over five delay scans of the maximum amplitude of the THz signal in the delay-time interval between 21 and 29 ps. In this delay-time interval, the first commensurate echo of the THz beam transmitted through CH_3F gas reaches its maximum (Fig. 4). This timing of the commensurate echo is quite specific for CH_3F, and thus enables the measurement of THz images of this gas with high contrast and chemical specificity.

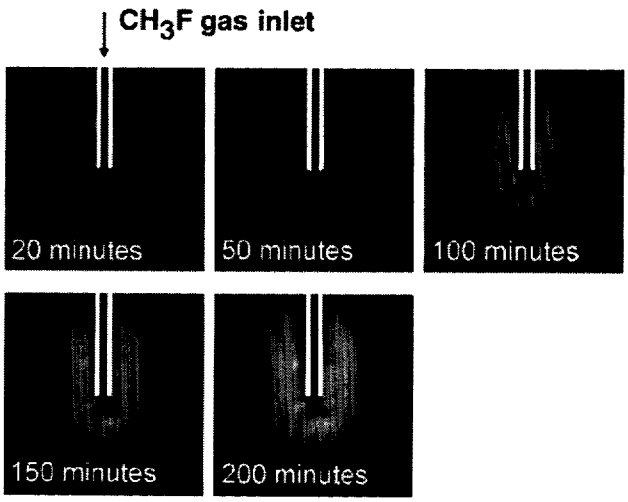

FIGURE 6 THz images at five different time delays showing the diffusion of CH_3F gas in polystyrene foam. Each image consists of 70 pixels × 70 pixels and has a size of 2.16 cm^2 × 2.16 cm^2. The signal at each pixel is obtained by taking the maximum amplitude of the first commensurate echo that is generated by the interaction of the THz light field with the rotational transitions of the CH_3F molecules

The specific timing of the commensurate echoes can be used to distinguish different chemical compounds contained in a mixture. The conventional method to distinguish a particular chemical substance would be to monitor the amplitude at a characteristic frequency. However, this latter method leads to a much lower signal to noise ratio. The essential advantage of using the timing of the commensurate echo is that a single characteristic frequency component is not used, but rather the *correlation* of many frequency components in the spectrum, which are all specific for a particular chemical compound.

4 Summary

We presented a setup that allows for the measurement of high-quality THz images. An essential feature of this setup is that the measurement time of each pixel of the image is strongly reduced by improving both the THz emission and detection. With water-cooled, wide-aperture, semi-insulating GaAs THz emitters that are biased with a 50-kHz square-wave ac bias voltage with an amplitude of 400 V, we can generate electric field strengths up to 98 V/cm and average THz powers of approximately 100 μW. Using this emitter in combination with rapid delay scanning and differential lock-in detection at 50 kHz, we obtain shot-noise-limited detection of THz transients. As a result, a THz transient with a large dynamic range of ~ 5000 can be measured in 20 ms.

We showed that the THz imaging setup can be used to reveal objects hidden in containers that are completely opaque to light at optical frequencies. We also demonstrated that the setup can be used to follow relatively slow processes like the diffusion of gases. In the latter case images of high quality and chemical specificity can be obtained by using the specific timing of the commensurate THz echoes that result from the coupling of the propagating THz light with the rotational resonances of these gases.

ACKNOWLEDGEMENTS This work was performed as part of the EU TERAVISION programme (IST-1999-10154). The research presented in this paper is also part of the research programme of the 'Stichting Fundamenteel Onderzoek der Materie (FOM)', which is financially supported by the 'Nederlandse Organisatie voor Wetenschappelijk Onderzoek (NWO)'. The work is also partially supported by the Netherlands Research Council for Chemical Sciences (NWO-CW).

REFERENCES

1 X.-C. Zhang, Y. Yin, X.F. Ma: Appl. Phys. Lett. **61**, 2764 (1992)
2 A. Nahata, A.S. Weling, T.F. Heinz: Appl. Phys. Lett. **69**, 2321 (1996)
3 A. Bonvalet, M. Joffre, J.L. Martin, A. Migus: Appl. Phys. Lett. **67**, 2907 (1995)
4 M. van Exter, D.R. Grischkowsky: IEEE Trans. Microwave Theory Tech. **38**, 1684 (1990)
5 J.T. Darrow, B.B. Hu, X.-C. Zhang, D.H. Auston: Opt. Lett. **15**, 323 (1990)
6 C. Weiss, R. Wallenstein, R. Beigang: Appl. Phys. Lett. **77**, 4160 (2000)
7 Q. Wu, X.-C. Zhang: Appl. Phys. Lett. **67**, 3423 (1995)
8 Q. Wu, X.-C. Zhang: Appl. Phys. Lett. **68**, 1604 (1996)

9 P.U. Jepsen, C. Winnewisser, M. Schall, V. Schyja, S.R. Keiding, H. Helm: Phys. Rev. E **53**, R3052 (1996)
10 Y. Cai, I. Brener, J. Lopata, J. Wynn, L. Pfeiffer, J.B. Stark, Q. Wu, X.-C. Zhang, J.F. Federici: Appl. Phys. Lett. **73**, 444 (1998)
11 H.J. Bakker, G.C. Cho, H. Kurz, Q. Wu, X.-C. Zhang: J. Opt. Soc. Am. B **15**, 1795 (1998)
12 G. Gallot, D. Grischkowsky: J. Opt. Soc. Am. B **16**, 1204 (1999)
13 Q. Chen, X.-C. Zhang: Appl. Phys. Lett. **74**, 3435 (1999)
14 G. Zhao, M. ter Mors, W.T. Wenckebach, P.C.M. Planken: J. Opt. Soc. Am. B **19**, 1476 (2002)
15 G. Zhao, R.N. Schouten, N. Valk, P.C.M. Planken, W.T. Wenckebach, P.C.M. Planken: Rev. Sci. Instrum. **73**, 1715 (2002)
16 H. Harde, R.A. Cheville, D. Grischkowsky: J. Opt. Soc. Am. B **14**, 3282 (1997)
17 H. Harde, S. Keiding, D. Grischkowsky: Phys. Rev. Lett. **66**, 1834 (1991)